

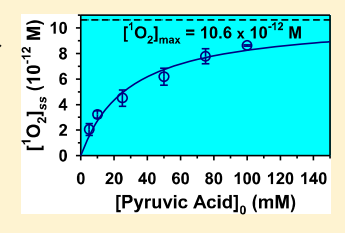
Production of Singlet Oxygen (${}^{1}O_{2}$) during the Photochemistry of Aqueous Pyruvic Acid: The Effects of pH and Photon Flux under Steady-State O_{2} (aq) Concentration

Alexis J. Eugene and Marcelo I. Guzman*

Department of Chemistry, University of Kentucky, Lexington, Kentucky 40506, United States

Supporting Information

ABSTRACT: The photochemistry of pyruvic acid (PA) in aqueous atmospheric particles contributes to the production of secondary organic aerosols. This work investigates the fate of ketyl and acetyl radicals produced during the photolysis ($\lambda \geq 305$ nm) of 5–100 mM PA under steady state $[O_2(aq)] = 260 \,\mu\text{M}$ ($1.0 \leq pH \leq 4.5$) for photon fluxes between 1 and 10 suns. The radicals diffuse quickly into the water/air interface of microbubbles and react with dissolved O_2 to produce singlet oxygen (${}^1O_2^*$). Furfuryl alcohol is used to trap and bracket the steady-state production of $2 \times 10^{-12} \leq [{}^1O_2^*] \leq 1 \times 10^{-11} \,\text{M}$. Ion chromatography mass spectrometry shows that 2,3-dimethyltartaric acid (DMTA), 2-(3-oxobutan-2-yloxy)-2-



hydroxypropanoic acid (oxo- C_7 product), and 2-(1-carboxy-1-hydroxyethoxy)-2-methyl-3-oxobutanoic acid (oxo- C_8 product) are formed under all conditions investigated. The sigmoidal dependence of initial reaction rates with pH resembles the dissociation curve of PA. For increasing photon fluxes, the branching ratio of products shifts away from the radical recombination that favors DMTA toward multistep radical chemistry forming more complex oxocarboxylic acids (oxo- C_7 + oxo- C_8). The large steady-state production of 1O_2 indicates that PA in aerosols can be a significant source of atmospheric oxidants on par with natural organic matter.

INTRODUCTION

The photo-oxidation of biogenic and anthropogenic emissions proceeds in the gas phase to generate large quantities of pyruvic acid (PA), 1-4 an abundant species in atmospheric organic aerosols. 5-7 Up to 67% of the formed molecules of gaseous PA can quickly partition into the aqueous phase of particles⁸ because of large Henry's law constant $(K_{\rm H} = 3.1 \text{ mol kg}^{-1} \text{ Pa}^{-1})$. The crystal structure of PA is almost planar with intermolecular interactions dominated by hydrogen bonding. 10 The reported reactive uptake coefficient of gaseous PA by water, $\gamma_{PA} = 0.06$, involves an interfacial accommodation with a perpendicular orientation of the molecular plane of PA to the surface normal.¹¹ In this configuration, the C=O group of PA participates in the uptake by undergoing cooperative reversible hydration, with an equilibrium constant $K_{\rm Hyd}$ = 2.10 at 25 °C, ¹² resulting in the formation of an UV-transparent gem-diol, 2,2-dihydroxypropanoic acid. 13 The conjugated C=O chromophore of PA is widely available in water to absorb sunlight and promote photoinduced reactions. 14-19 The estimated rate of production of PA in atmospheric waters is 1.80 $(\pm 0.46) \times 10^{9}$ mol year⁻¹.²⁰

The photochemical loss of fully dissociated PA at pH 6.1 (p K_a = 2.39), ²¹ that is, for a molar fraction of pyruvate $\alpha_{PA}^{-} \ge 0.99$, is an order of magnitude lower than that of undissociated PA. ²² The suppression of the photoreaction at high pH has been attributed to the unavailability of hydrogen in the carboxylic group for abstraction, ²³ even though such a target for abstraction is unlikely and despite the fact that $-CH_3$ groups are still readily available at high pH. In contrast, the lower gem-diol to carbonyl ratio in equilibrium for pyruvate results in greater absorption than that for PA, ²⁴ suggesting an enhancement in photoactivity

should be expected at such pH \geq p K_a + 2. The unpredicted photoreactivity changes with pH of PA^{22,24} demand a systematic study of the reaction under speciation conditions that cover the range of molar fractions $\alpha_{PA} = 1$ and $\alpha_{PA}^- = 1$, for the acid and base, respectively. Therefore, this work aims to provide a comprehensible and quantitative study of the effect of pH on the decay of PA and on the formation of each photoproduct identified in our previous work; 16 these products are 2,3dimethyltartaric acid (DMTA), 2-(3-oxobutan-2-yloxy)-2-hydroxypropanoic acid (named the oxo-C7 product), 2-(1carboxy-1-hydroxyethoxy)-2-methyl-3-oxobutanoic acid (named the oxo-C8 product), and acetic acid. Three recommendations are followed: (1) Utilizing a well-purified starting material to avoid confusion with products from impurities. 16,17 (2) Employing methods that eliminate any possible overlap of each major analyte. 16,17 (3) Operating an experimental setup optimized to work under a constant dissolved oxygen level, for example, at $[O_2(aq)] = 260 \mu M$ at 25 °C for equilibrium conditions between water and air without creating hypoxia.²⁵

In addition to reporting the photoprocessing of PA at variable pH equilibrated with air, 13,16,17,25 the effect of other in situgenerated oxidizers is explored. There is no previous report dealing with the reactivity of singlet oxygen ($^{1}O_{2}^{*}$) and the excited state of molecular oxygen, during the photochemistry of

Received: June 25, 2019
Revised: September 8, 2019
Accepted: September 24, 2019
Published: September 24, 2019

aqueous PA. In atmospheric waters, ¹O₂* can be supplied either from the gas phase after partitioning or from photochemical reactions within the aqueous particles.²⁶ The photochemical formation of ¹O₂* requires energy transfer from a triplet exited state of an organic molecule to ground-state O2. In water, under air saturated conditions and sunlight, the photoexcited triplet state of PA (${}^{3}PA^{*}$) should form a significant amount of ${}^{1}O_{2}^{*}$. Past measurements in atmospheric waters including unidentified chromophores for the fall season have bracketed the range of $[{}^{1}O_{2}^{*}(aq)] = 2.7 \times 10^{-14} - 1.1 \times 10^{-12} \text{ M}, {}^{27} \text{ with an average in}$ winter of $2.6 \times 10^{-13} \text{ M.}^{26}$

Nevertheless, there are no data regarding ¹O₂* photoformation and its effect in irradiated waters where PA is mixed with other markers of atmospheric pollution. Although ¹O₂* is typically a minor sink for refractory compounds in atmospheric waters, electron-rich species such as furans [i.e., furfuryl alcohol (FFA)] emitted during biomass burning^{28,29} can be especially susceptible to the attack by this oxidizer. Therefore, two major objectives are needed to advance the understanding of the photochemistry of PA in atmospheric waters. The first objective is to measure the rate of formation of the previously identified photoproducts under variable pH and photon flux for steadystate $[O_2(aq)]_{ss} = 260 \,\mu\text{M}$. The second objective is to investigate the formation of ${}^{1}O_{2}^{*}$ using FFA (a marker of biomass burning emissions) under relevant tropospheric conditions.

■ EXPERIMENTAL SECTION

Preparation of Experiments. All the reactions were performed in duplicate using fresh solutions prepared before each photolysis of PA (Sigma-Aldrich, 98.5%, freshly distilled under vacuum) dissolved in ultrapure water (18.2 M Ω cm⁻¹, ELGA PURELAB Flex, Veolia). The plots report the average value from these experiments with the corresponding standard deviation as error bars (even though they could be smaller than the symbols shown). The choice of working concentrations was described in detail previously; in brief, it was estimated that acidic aqueous urban aerosols may contain 5-200 mM PA. 13,16,30 The pH of solutions was adjusted by adding hydrochloric acid (EMD, 37.7%) or sodium hydroxide (AMRESCO, 99.0%) and measured using a calibrated pH electrode (Orion, Thermo Scientific). A 200 mL aliquot of the pH-adjusted solution was transferred to a 220 mL quartz photochemical reactor equipped with a jacket for temperature control (described previously).³¹ The solution in the photoreactor was sparged at a flow rate of 2.0 mL min⁻¹ in the dark with air through a 25 μ m internal diameter (ID) coarse glass frit starting 30 min prior to photolysis. Monitoring of $[O_2(aq)]$ during the reactions was carried out by a polarographic oxygen probe (Thermo Orion, 081010MD) calibrated at maximum saturation in an air-calibration sleeve and at 0% saturation in a saturated sodium sulfite/CoCl₂ solution. In opposition to previous studies, ^{22,23} this is the first time that the effects of pH and the absorbed photon rate on the photochemistry of aqueous PA are systematically studied under steady-state dissolved O2

Photochemical Conditions. The solutions were irradiated with a 1.0 kW Xe-Hg lamp filtered through (1) water, (2) a cutoff filter at $\lambda \geq 305$ nm, and (3) only for the selected experiments (as indicated in the corresponding caption to figures), neutral density filters to attenuate the photon flux of the lamp to 67.19, 32.45, 21.50, or 10.56% of the total. 16-18,31-Chemical actinometry using phenylglyoxylic acid³⁶ was used to measure the incident photon flux of the full lamp and at each of

the attenuated intensities in the absorption region $305 \le \lambda \le 420$ nm, as described previously.²⁵ The effective incident photon fluxes, I_0 , reported were obtained after correcting the actinometric measurement by comparing the convoluted spectra of phenylglyoxylic acid with the lamp versus PA with the lamp. The full photon flux used in this work (without attenuation) was I_0 = $1.13 (0.03) \times 10^{-5}$ einstein L⁻¹ s⁻¹. The quantum yields reported correspond to the ratio of the initial reaction rates to the absorbed photon flux, I_a , which is calculated from eq 1

$$I_{a} = I_{0}(1 - e^{-2.303\epsilon l[PA]_{0}})$$
 (1)

where $\varepsilon = 11.3 \text{ M}^{-1} \text{ cm}^{-1}$ is the molar absorption coefficient of PA at $\lambda_{\text{max}} = 321$ nm, l = 4.50 cm is the reactor path length, and the initial PA concentration is given by $[PA]_0$.

Equation 1 stipulates that light absorption and therefore the photolysis rate of this reaction vary linearly 16 with [PA]0 only below ~ 1 mM for l = 4.5 cm. The previous important concept 13,16 should have been considered in the UV-visible spectroscopy work about PA photochemistry³⁷ to avoid inference-observation confusion. However, for $1 < [PA]_0 <$ 300 mM, the photolysis rate must decrease as the rate of photon absorption drops. During irradiation, the solutions were maintained at 25 °C and magnetically stirred while being continuously sparged with air. Aliquots (5 mL) were removed from the reactor at regular intervals and analyzed immediately.

Analysis of Products. Organic products were quantified by ion chromatography mass spectrometry (IC-MS) using a Dionex ICS-2000 ion chromatograph (IonPack AS11-HC, 2 mm column) equipped with a conductivity detector and an electrospray ionization (ESI) mass spectrometer (Thermo Scientific MSQ Plus) operating in the negative mode as described previously. 16 The samples were diluted 200 times in ultrapure water before injection onto the IC column. Quantification was performed using commercially available standards for pyruvate (JT Baker, 99.4%) and acetate (EM Science, 99.0%). For products that were unavailable, quantitative ¹H nuclear magnetic resonance (qNMR) was used to calibrate the relative response factor in MS. 16,38 These relative response factors were determined by analyzing the same set of fresh samples by both qNMR and IC-MS. ¹H NMR integrals provide concentrations from the number of hydrogen atoms yielding the signal, which allowed the correction of MS calibrations using pseudostandards for the unavailable compounds as previously described. All the reaction rates reported correspond to initial rates, which are linear unless otherwise specified.

Quantification of ¹O₂. FFA (Alfa Aesar, 99.1%), an abundant biomass burning molecule emitted during biomass burning, was used in experiments measuring singlet oxygen (¹O₂) production. A spike of FFA was added to the solution of PA immediately before photolysis ($[FFA]_{final} = 1.20 \text{ mM}$). The decay of FFA was followed by high-pressure liquid chromatography (HPLC) (Agilent 1100) using an Agilent XDB-C18 column (5 μ m, 4.6 × 150 mm) with UV detection at λ = 218 nm. Samples were injected (25.0 μ L) in the undiluted form into the column. A flow rate of 1.0 mL min⁻¹ for mixing solvent A made of 10.0 mM formate buffer (sodium formate, Acros, 99.9%; formic acid, Fisher Optima LC/MS, 99.5%) at pH 3.0 with solvent B made of acetonitrile (EMD Millipore LC/MS, 99.99%) was employed. Gradient elution allowed FFA to be separated from PA and the photolysis products by using initially 5% solvent B for 3 min, then ramping to 25% solvent B over 5 min, and holding at 25% solvent B for 1 min. The steady-state

singlet oxygen concentration, [1O2]ss, was calculated by dividing the experimental rate constant determined in this work by the recommended value for $k_{^{1}\mathrm{O},+\mathrm{FFA}} = 1.08 \times 10^{8} \,\mathrm{M}^{-1} \,\mathrm{s}^{-1}$, which is corrected for temperature and salt content.³⁹ The experimental rate constant was obtained from the slope of a linear plot of $ln([FFA]_t/[FFA]_0)$ versus time for the first-order decay process. Figure S1 (Supporting Information) displays an example of this procedure. No new chromatographic peaks for hypothetical adducts (i.e., of either PA or its photolytic radicals with FFA) could be observed, discarding their direct reactivity

Monitoring of Hydroxyl Radicals (HO*). The hypothetical production of HO is explored while monitoring photoreactions spiked to [benzoic acid]_{final} = $1.06 \text{ mM}^{26,40}$ or [terephthalic acid]_{final} = 0.50 mM.⁴¹ Detailed information for this method is available in the Supporting Information. In brief, the production of HO[•] can be disregarded during PA photolysis. The concentrations of benzoic and terephthalic acids remained constant during irradiation experiments in the presence of each HO[•] trap (Figure S2, Supporting Information).

■ RESULTS AND DISCUSSION

Time Series of PA Loss and Product Formation. Figure 1 shows the ion chromatography separation before and after 1 h

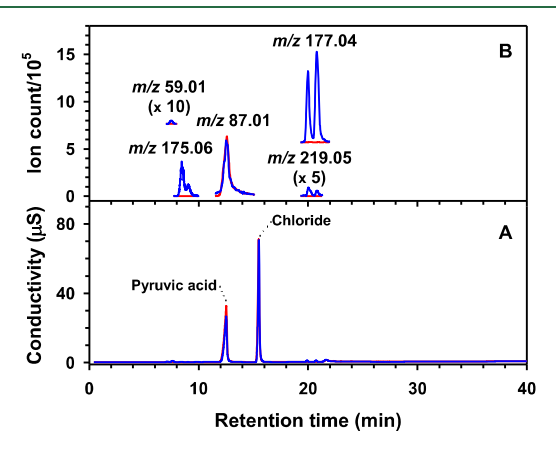


Figure 1. (A) Ion chromatogram with total conductivity detection of 100.0 mM PA at pH 1.0 and 25 °C (red) before and (blue) after 1 h photolysis ($\lambda \ge 305$ nm) under continuous air sparging through a 25 μ m ID frit at 2.0 mL min⁻¹ for an effective photon flux $I_a = 1.13 \times 10^{-5}$ einstein L⁻¹ s⁻¹. The use of HCl for pH adjustment causes the presence of a chloride peak. (B) IC-ESI(-)/MS-extracted ion chromatograms for the same experiment in panel A for PA (m/z 87.01), DMTA (m/z177.04), the oxo- C_7 product (m/z 175.06), the oxo- C_8 product (m/z 175.06)219.05), and acetic acid (m/z 59.01).

photolysis ($\lambda \ge 305$ nm) of 100.0 mM PA at pH 1.0 for the full photon flux under continuous air sparging, which ensures that the reaction reported occurs under a constant $[O_2(aq)] = 260$ (± 7) μ M. The data in Figure 1B display the extracted ion chromatograms in the negative ionization mode for the reactant PA at a mass-to-charge ratio (m/z) (m/z) of 87.01 and the main photoproducts. The chromatographic peaks of photoproducts registered at m/z 177.04, 175.06, 219.05, and 59.01 are for DMTA, 2-(3-oxobutan-2-yloxy)-2-hydroxypropanoic acid (named the oxo-C₇ product), 2-(1-carboxy-1-hydroxyethoxy)-2-methyl-3-oxobutanoic acid (named the oxo-C₈ product), and acetic acid, respectively. 16,1

The structures of these products are shown in the mechanism of Scheme 1. The two chromatographic peaks for each heavier product than PA are attributed to separable pairs of diastereomers formed in a radical coupling process, yielding molecules with more than one chiral center. ^{16,35} In agreement with our report for a radical mechanism, ^{16,17} under all sets of conditions used here, the same products are observed, albeit in different ratios.

Figure 2 shows the typical photoreaction kinetics under continuous air saturated conditions. The trace for $[O_2(aq)]$ versus time (external axes of Figure 2) demonstrates that the setup was optimized to always maintain air saturated conditions. The first-order decay of PA fits an exponential function with a rate constant, $k_{\rm PA} = 7.43 \times 10^{-5} \, {\rm s}^{-1}$, and a coefficient of determination, $r^2 = 0.995$. The concentrations of (in the order of abundance) DMTA, the sum for the oxo-C₇ and oxo-C₈ products, and acetic acid increase exponentially according to the equation

$$[Product] = [product]_{\infty} (1 - e^{-k_f t})$$
 (2)

where $[product]_{\infty}$ is a constant representing the asymptotic upper limit that would be reached as the time $t \to \infty$ and k_f is the formation rate constant (both given in Table 1). All the nonlinear fittings in Figure 2 have $r^2 \ge 0.993$. The stoichiometric conversion factors of 2, 1, and 3 molecules of PA needed to produce 1 molecule of DMTA, acetic acid, and the oxo-C₇ + oxo-C₈ products, respectively, allow for closing the mass balance after 1 h of irradiation as shown in Figure 2. In addition, based on the stoichiometry of each product to the number of PA molecules consumed, 16 the predicted [product] $_{\infty}$ in Table 1 can explain up to 95.7% of the mass balance as $t \to \infty$, which demonstrates an excellent understanding of the photoreaction based on these products. Similarly, the mass balance measured at the final time (1 h) can explain 96.1% of the conversion of PA. Therefore, the stoichiometric factors employed are verified to be correct. In consequence, any missing products are quantitatively negligible (or any possible missing minor products are at the level of traces).

A past research work using a reactor with a shorter path length has demonstrated the exponential behavior, 16 described above for Figure 2. Therefore, the linear appearance of the trends in Figure 2 is only a consequence of determining most concentration points during the early decay of PA. For the airsaturated conditions corresponding to Figure 2 ($[O_2(aq)]_{ss}$ = 260 μ M), the kinetics of the reaction are truly controlled by the initial [PA]₀. Thus, valuable information is provided in Figure 2 to mimic the photolytic process under realistic atmospheric conditions. This work improves our previous findings 16 (for small amounts of [O₂(aq)] remaining) and shows a higher production of DMTA than the oxo- C_7 + oxo- C_8 products in the presence of $[O_2(aq)]_{ss}$ = 260 μ M. Similarly, the valuable k_f parameters reported for DMTA and the oxo-C₇ + oxo-C₈ products (Table 1) are an order of magnitude smaller than that in our previous report, 16 which is consistent with the scavenging effect oxygen has on the generated radicals.

Upon irradiation of PA (reaction R1a, Scheme 1), a singlet excited state is produced that undergoes intersystem crossing (ISC) forming the triplet ³PA* (reaction R1b). This ³PA* is thermally lost, regenerating ground-state PA (reaction R2) with a spontaneous decay rate constant $k_{\rm R2} = 2 \times 10^6 \, {\rm s}^{-1}$, or reacts with ground-state PA (overall reaction R3) via proton-coupled electron transfer (PCET) to yield two intermediate radical species, K^{\bullet} and an acyloxyl radical $(X^{\bullet})^{16}$ The formation of the

Scheme 1. Proposed Mechanism for the Photochemistry of Aqueous PA in the Presence of Dissolved Oxygen, O₂(aq)^a

"Adapted from A. J. Eugene and M. I. Guzman, in "Reactivity of ketyl and acetyl radicals from direct solar actinic photolysis of aqueous pyruvic acid", J. Phys. Chem. A, 2017, 121, 15, 2924–2935. 16 Copyright 2017 American Chemical Society.

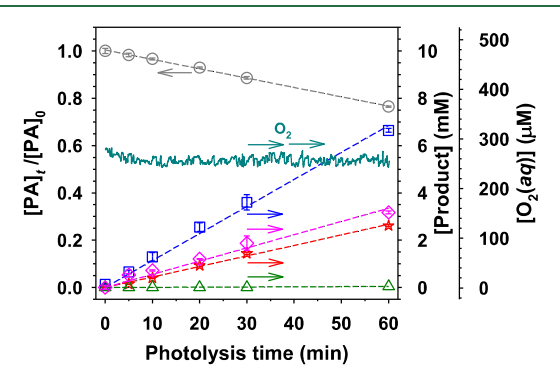


Figure 2. Kinetics of (gray circle) PA decay and formation of (blue square) DMTA, (pink diamond) acetic acid, (red star) the oxo-C₇ product, and (green triangle) the oxo-C₈ product for the same experiment in Figure 1. The external axes is displayed for the teal trace of $[O_2(aq)]$ vs time.

products is not stopped in air-saturated solutions ($[O_2(aq)]$ = 260 μ M) or in the presence of [2,2,6,6-tetramethylpiperidin-1-oxyl] = 2 mM, a radical scavenger. ^{13,16,25} For the reactant conversion reported (<30%), PA is always the dominant absorbing chromophore, producing $^3\text{PA*}$ that is quenched by ground-state PA itself $(k_\text{Q}=2\times10^8~\text{M}^{-1}~\text{s}^{-1})^{42}$ at the working

Table 1. Exponential Growth Parameters in Eq 2 for the **Products in Figure 2**

| | $[product]_{\infty} \ (mM)$ | $k_{\rm f}~({ m s}^{-1})$ |
|------------------------------|-----------------------------|---------------------------|
| DMTA | 20.4 | 1.10×10^{-4} |
| acetic acid | 6.31 | 1.94×10^{-4} |
| $oxo-C_7 + oxo-C_8$ products | 16.2 | 4.96×10^{-5} |

concentrations. Thus, a dominant bimolecular initiation mechanism (reaction R3) occurs with a rate that exceeds spontaneous decay (reaction R2).¹³

The acyloxyl radical X* decarboxylates quickly and irreversibly to form Y (reaction R4a), which most likely gets hydrated (reaction R4b). Bimolecular reactions R5a and R7a indicate how K[•] and Y[•] are converted into their respective peroxyl radicals in the presence of O₂(aq). Reactions R5b and R7b result in the formation of PA and acetic acid, respectively, while reaction R6 produces DMTA from the recombination of K* + K*. Reactions R8 and R9 account for the respective production of the oxo-C₈ and oxo-C₇ products. Although reactions R1-R9 were discussed in detail previously, 16 reaction R10 describes the in situ generation of singlet oxygen during PA photolysis as a new pathway introduced here.

Experiments under Excess Dissolved O2. A previous report utilized a 1.6 mm ID single orifice sparger, 25

demonstrating the importance of properly controlling the mass transfer of $O_2(g)$ into water. Notably, the rate-determining step of the entire photoprocess is controlled by an interfacial reaction following a Langmuir isotherm, which can result in the creation of hypoxic conditions.²⁵ In order to fully characterize the photolytic system operating under nonlimited mass transfer of $O_2(g)$ to water, the experiments in this work are optimized employing a 25 μ m ID frit sparger. The 25 μ m ID frit sparger allows for a true excess O₂(aq) environment to be achieved by increasing the interfacial area available for O2(g) to diffuse across, which increases the efficiency of mass transfer for the reactor. This frit allows for smaller bubbles of gas to be created to improve the surface area to volume ratio, compared to the use of a larger 1.6 mm ID sparger, ²⁵ enhancing O₂(g) molecules' access to the gas-liquid interface. Complete O₂(aq) saturation throughout the 1 h irradiation period even for 100 mM PA solutions is achieved here. In other words, the system was optimized for keeping a constant $[O_2(aq)] = 260 \,\mu\text{M}$ during the full irradiation period. The optimized conditions under $O_2(aq)$ excess also enable a kinetically simplified description of the system to explore the effects of other parameters, namely, pH and I_a on photoreaction. Additionally, the significance of the reaction of the photogenerated radicals from PA with $O_2(aq)$ becomes even more apparent than that previously reported. The overall process starts with the homogeneous photoproduction of carbon-centered radicals, which quickly diffuse into the air/water interface of bubbles to bimolecularly react with O₂-forming products that are desorbed from this interface and diffuse away.

Effect of pH under Excess Dissolved O₂. Figure 3 shows how the initial reaction rates of PA loss and production of

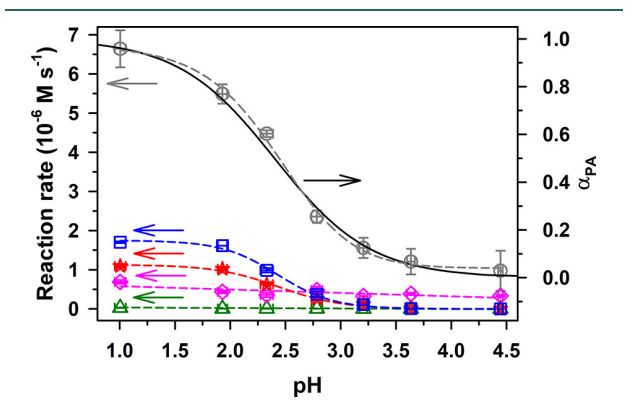


Figure 3. Initial reaction rate of (gray circle) PA decay and production of (blue square) DMTA; (red star) oxo-C₇ product; (pink diamond) acetic acid; and (green triangle) oxo- C_8 product during irradiation at λ \geq 305 nm of 100.0 mM solutions of PA at 25 °C and variable initial pH with constant (nondepleted) air sparging of 2.0 mL min⁻¹ through a 25 µm ID frit. Dashed lines represent nonlinear sigmoid fittings to experimental data. The solid black line corresponds to the dissociation fraction of PA (α_{PA}) calculated based on p K_a = 2.39 in ref 21.

DMTA and the oxo-C₇ product closely resemble sigmoidal dependence on pH for the speciation of PA (p $K_a = 2.39$). From the second derivative of each sigmoid (for PA, DMTA, and the oxo- C_7 product), the average inflection point is pH = 2.42 (± 0.01), which is within the experimental error from the pK_a of PA. Although the oxo-C₈ product trend drops with increasing pH in Figure 3, the reaction rates are very small (because of its unstable behavior as a β -ketocarboxylic acid that

favors decarboxylation) to evaluate an inflection point from the data. These low reaction rates for the oxo-C₈ product are consistent with a near-barrierless concerted β -ketocarboxylic acid decarboxylation to form the oxo-C₇ product, involving proton transfer (-COOH O= C_{β}) and C-C bond-scission, releasing CO₂ from (initially) quaternary carbon. 15,44 The behavior of acetic acid does not follow a sigmoid to be associated with a dependance on pH.

The results in Figure 3 support a clear photoreactivity dependence on the availability of protons, which determines the amount of undissociated acid as the key participant in the ratelimiting step rather than on available pyruvate. This finding is consistent with the results of kinetic isotope effect (KIE) experiments using D₂O as the solvent, ¹⁶ where the acidic hydrogen of PA is essentially replaced with deuterium. The large primary KIEs observed for all the products could only be rationalized as resulting from the acidic proton being involved in the key step of each product formation. Thus, the formation of the initial radical species is controlled in the mechanism (i.e., reaction R3a, Scheme 1) by the formation of an excited state from undissociated PA. Although the excited state from the dissociated form could be promoted upon irradiation, pyruvate lacks its acidic proton for completing PCET that creates K* and X^o radicals.⁴

After ISC, the produced ³PA* can interact directly with a ground-state PA molecule (overall reaction R3a-c, Scheme 1). The transfer from the -COOH of PA to $^3PA^*$ in a PCET mechanism could proceed through a six-member ring transition state with the electron transfer involving C=O moieties. Considering that a typical C-H bond is 58.6 (± 0.1) kJ mol⁻¹ weaker than a O-H bond, 46 if pure hydrogen atom abstraction were to occur, the -CH₃ group of PA would be the preferred source over either its -COOH group or one of the hydroxyl hydrogens from 2,2-dihydroxypropanoic acid (the more abundant gem-diol form of PA in equilibrium). However, the PCET process should be energetically more favorable than hydrogen abstraction from the -CH₃ group because the formed metastable radical \boldsymbol{X}^{\bullet} decarboxylates exothermically (reaction R4a). 13-15 In agreement with this interpretation, the proton transfer from the -COOH group has also been calculated to be more favorable than from the -CH3 groups for the case of PA clusters formed during supersonic expansion subjected to electron ionization with 70 eV electrons or photoionization with UV photons at 193 nm. 47

Effect of Photon Flux under Excess Dissolved O₂. Figure 4 demonstrates that the initial reaction rates scale linearly with the absorbed photon flux. Because the photochemical quantum yields (Φ) are calculated as the ratio of the initial reaction rates to the absorbed photon flux, the slopes for each linear regression line (Figure 4) directly reflect the experimental values of Φ listed in Table 2. The reported Φ values allow for the comparison of the photoreaction across different studies under excess dissolved O2 and serve as an input parameter for atmospheric models aiming to improve the understanding of aqueous processing of organic molecules.

Based on the proposed mechanism in Scheme 1, 16 one, two, and three PA molecules are needed to form one molecule of acetic acid, DMTA, and the oxo-C₇ + oxo-C₈ products, respectively. A weighted sum taking into account the stoichiometry of the respective products' quantum yields in Table 2 results in a total value of 0.62 (\pm 0.04), which is within the error of the corresponding overall Φ measured for the loss of PA of 0.58 (± 0.02). Therefore, the four products of interest

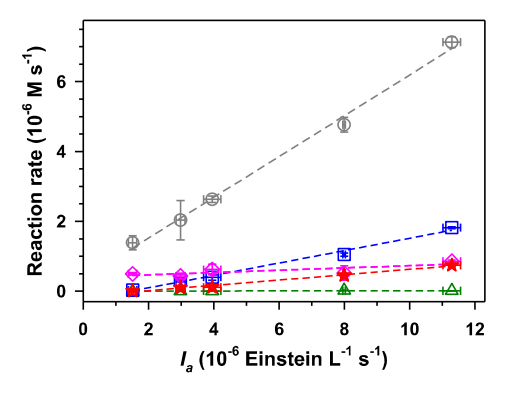


Figure 4. Reaction rate of (gray circle) PA decay and production of (blue square) DMTA; (red star) oxo- C_7 product; (pink diamond) acetic acid; and (green triangle) oxo- C_8 product during irradiation at $\lambda \ge 305$ nm of 100.0 mM PA solutions at pH 1.0 and 25 °C with constant (nondepleted) air sparging (2.0 mL min⁻¹) through a 25 μ m ID frit for variable absorbed photon flux (I_a).

Table 2. Quantum Yields (Φ) under Excess $O_2(aq)$ Calculated from the Slopes in Figure 4

| species | Φ |
|----------------------------|----------------------------------|
| PA | $5.8 (\pm 0.2) \times 10^{-1}$ |
| DMTA | $1.8 \ (\pm 0.1) \times 10^{-1}$ |
| oxo-C ₇ product | $7.6 (\pm 0.4) \times 10^{-2}$ |
| oxo-C ₈ product | $1.5 \ (\pm 0.7) \times 10^{-3}$ |
| acetic acid | $3.2 (\pm 0.1) \times 10^{-2}$ |

account for the vast majority, if not all, of PA lost under excess $O_2(aq)$.

Even though the reaction rates scale linearly with increasing photon flux as shown in Figure 4, the distribution of products observed is enhanced for the complex $oxo-C_7 + oxo-C_8$ products. Figure 5 highlights the previous observation by

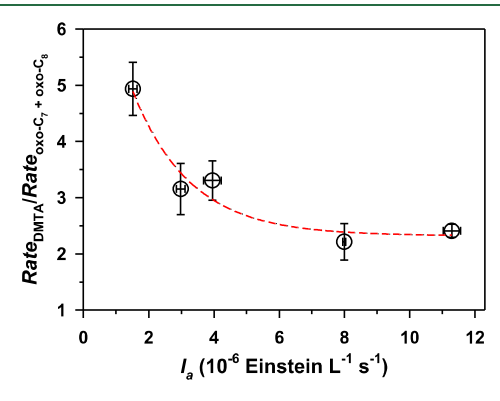


Figure 5. Branching ratio calculated as the rate of DMTA (rate_{DMTA}) production over the sum of the production rates of the two oxocarboxylic acid products ($\operatorname{rate}_{\operatorname{oxo-C_7+oxo-C_8}}$) at variable absorbed photon flux (I_a) by the solution. All the data are derived from Figure 4.

showing the dependence of the ratio of the initial reaction rate of products (for the formation of DMTA, rate_{DMTA}, and the oxo- C_7 + oxo- C_8 products, rate_{oxo- C_7 +oxo- C_8}) with I_a . The oxocarboxylic acid branch of the mechanism (reactions R8 and R9, Scheme 1) grows faster than the channel for DMTA production (reaction R6) for larger absorbed photon fluxes. Such a behavior can be explained by the increased conversion of PA at higher I_a and by

the requirement of three PA molecules for producing the oxocarboxylic acid products while DMTA requires only two. The ratio ${\rm rate_{DMTA}/rate_{oxo-C_7+oxo-C_8}}$ reaches a maximum of 4.9 at low photon flux and decays exponentially to level out at ~2.3 for medium and high photon fluxes (Figure 5). Importantly, the branching ratio value of ~2.3 is obtained from the ratio of (1) the quantum yields in Table 2 and (2) the first-order rate constants in Table 1. Thus, from the ratio ~2.3 and the rate constant for the formation of DMTA (reaction R6, Scheme 1), $k_{\rm R6} = 2.0 \times 10^9~{\rm M}^{-1}~{\rm s}^{-1}$, an estimate of the combined rate constant for formation of the oxocarboxylic acid (oxo-C₈ + oxo-C₇) products of ~8.7 × $10^8~{\rm M}^{-1}~{\rm s}^{-1}$ is found.

Atmospheric Significance of Reactions Involving $O_2(aq)$. Our previous work has reported that as much as 90% of the photoproduced K^{\bullet} radicals are recycled back into PA by $O_2(aq)$. The null cycle that could regenerate PA has been supported by electron spin resonance measurements, optimizing the saturation signal of the radical generation at a fixed photon flux. In mixed aqueous aerosols, this pathway should provide a potentially large amount of alkyl peroxy radical (RO_2^{\bullet}) intermediates $(e.g., KO_2^{\bullet})$ of central importance for driving oxidation reactions with other available species. In addition to forming the alkyl (R^{\bullet}) and RO_2^{\bullet} radicals that are so important to atmospheric chemistry, PA irradiated in the presence of $O_2(aq)$ also forms O_2^{\bullet} . Figure 6 shows how irradiation of PA in

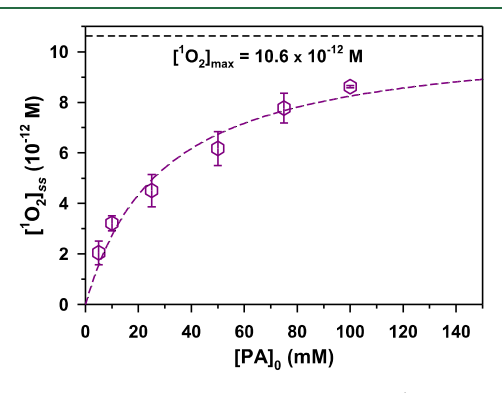


Figure 6. Steady-state singlet oxygen production, $[^{1}O_{2}]_{ss}$, during 1 h irradiation at $\lambda \geq 305$ nm $(I_{a}=1.13\times 10^{-5} \text{ einstein L}^{-1} \text{ s}^{-1})$ of airsaturated PA solutions at pH 1.0 and 25 $^{\circ}$ C under continuous air sparging through a 25 μ m ID frit.

atmospheric aerosols can produce significant steady-state concentrations of ¹O₂*. The values reported in Figure 6 vary with the concentration of PA used in the range $[^{1}O_{2}]_{ss} = 2.05 \times$ $10^{-12} - 8.62 \times 10^{-12}$ M for a photon flux equivalent to that provided by an irradiation of 10 suns. For comparison, studies from irradiated dissolved organic matter (DOM) collected from fog samples produced $[^{1}O_{2}]_{ss}$ on the order of 10^{-13} M for winter solstice levels of photons. The increase of $[^{1}O_{2}]_{ss}$ with $[PA]_{0}$ follows an hyperbolic behavior with a maximum $[^{1}O_{2}]_{max} = 1.06$ \times 10⁻¹¹ M under this set of conditions. Scaling down the previous concentration to the photon rate provided by 1 sun ($[^{1}O_{2}]_{max,lsun} \approx 1.06 \times 10^{-12} \text{ M}$) indicates that the potential production of ¹O₂ is equivalent to the maximum values reported by chromophores present in atmospheric waters.²⁷ This large $[^{1}O_{2}]_{ss}$ indicates that PA in aerosols can be a significant source of atmospheric oxidants on par with natural organic matter. Even after discounting the larger photon flux, the production of singlet oxygen by irradiated $5.0 \le [PA] \le 100.0$ mM demonstrates that 2-oxocarboxylic acids can contribute from 2 to 9 times more

[1O2]ss than the diverse mixture of DOM found in fog.50 Furthermore, this result suggests that under solar irradiation of aerosols containing PA, the chromophore can enhance the destruction of the aromatic products from biomass burning that are particularly susceptible to the reaction with ${}^{1}O_{2}^{*}$.

This work demonstrates the importance of performing photochemical experiments under adequate oxygenation conditions. We have shown that PA, rather than pyruvate, is the photoactive species required to produce the oligomeric products, 13,16 namely, DMTA and the oxo-C₇ and oxo-C₈ products, which provides additional indication that the initial reactive step proceeds through PCET. Concentrations of PA from 5 to 100 mM are capable of generating 2-9 times more [1O2]ss than irradiated field samples of natural fog waters. Furthermore, under solar irradiation, PA is so reactive toward $O_2(aq)$ that some coarse-mode aerosols (diameter > 14 μ m) may be oxygen-depleted environments, where different radical chemistry can take place. Finally, any aerosol rich in 2oxocarboxylic acid groups generating triplets should possess an enhanced oxidation capacity because of the photogeneration of ¹O₂* and RO₂* radicals.

ASSOCIATED CONTENT

S Supporting Information

The Supporting Information is available free of charge on the ACS Publications website at DOI: 10.1021/acs.est.9b03742.

Additional experimental details on HO monitoring; decay of FFA during the photolysis; and concentration of the hydroxyl radical trap (PDF)

AUTHOR INFORMATION

Corresponding Author

*E-mail: marcelo.guzman@uky.edu. Phone: (859)323-2892.

Marcelo I. Guzman: 0000-0002-6730-7766

Notes

The authors declare no competing financial interest.

ACKNOWLEDGMENTS

M.I.G. thanks the U.S.A. National Science Foundation for research funding under awards 1903744 and 1255290. A.J.E. acknowledges support by the NASA Earth and Space Science Fellowship (NESSF) Program.

ABBREVIATIONS

| PA | pyruvic acid |
|------|---------------------------|
| DMTA | 2,3-dimethyltartaric acid |

furfuryl alcohol **FFA** ¹O₂* singlet oxygen Φ quantum yield **ISC** intersystem crossing $k_{\rm f}$ formation rate constant $K_{\rm H}$ Henry's law constant

hydration equilibrium constant K_{Hyd} KIĖ kinetic isotope effect K^{\bullet} ketyl or lactic acid radical

PCET proton-coupled electron transfer

 Y^{\bullet} acetyl radical steady state

oxo-C₈ product 2-(1-carboxy-1-hydroxyethoxy)-2-methyl-3-

oxobutanoic acid

oxo-C₇ product 2-(3-oxobutan-2-yloxy)-2-hydroxypropanoic

acid

R* any alkyl radical RO2° any alkyl peroxy radical

REFERENCES

- (1) Carlton, A. G.; Turpin, B. J.; Lim, H.-J.; Altieri, K. E.; Seitzinger, S. Link between isoprene and secondary organic aerosol (SOA): Pyruvic acid oxidation yields low volatility organic acids in clouds. Geophys. Res. Lett. 2006, 33, L06822.
- (2) Lim, H.-J.; Carlton, A. G.; Turpin, B. J. Isoprene forms secondary organic aerosol through cloud processing: Model simulations. Environ. Sci. Technol. 2005, 39, 4441-4446.
- (3) Pillar, E. A.; Guzman, M. I. Oxidation of substituted catechols at the air-water interface: Production of carboxylic acids, quinones, and polyphenols. Environ. Sci. Technol. 2017, 51, 4951-4959.
- (4) Pillar-Little, E.; Guzman, M. An overview of dynamic heterogeneous oxidations in the troposphere. Environments 2018, 5, 104.
- (5) Fu, H.; Liu, H.; Mao, J.; Chu, W.; Li, Q.; Alvarez, P. J. J.; Qu, X.; Zhu, D. Photochemistry of dissolved black carbon released from biochar: Reactive oxygen species generation and phototransformation. Environ. Sci. Technol. 2016, 50, 1218-1226.
- (6) Kawamura, K.; Tachibana, E.; Okuzawa, K.; Aggarwal, S. G.; Kanaya, Y.; Wang, Z. F. High abundances of water-soluble dicarboxylic acids, ketocarboxylic acids and α -dicarbonyls in the mountaintop aerosols over the North China Plain during wheat burning season. Atmos. Chem. Phys. 2013, 13, 8285-8302.
- (7) Mkoma, S. L.; Kawamura, K. Molecular composition of dicarboxylic acids, ketocarboxylic acids, α -dicarbonyls and fatty acids in atmospheric aerosols from Tanzania, East Africa during wet and dry seasons. Atmos. Chem. Phys. 2013, 13, 2235-2251.
- (8) Bao, L.; Matsumoto, M.; Kubota, T.; Sekiguchi, K.; Wang, Q.; Sakamoto, K. Gas/particle partitioning of low-molecular-weight dicarboxylic acids at a suburban site in Saitama, Japan. Atmos. Environ. **2012**, 47, 546-553.
- (9) Saxena, P.; Hildemann, L. M. Water-soluble organics in atmospheric particles: A critical review of the literature and application of thermodynamics to identify candidate compounds. J. Atmos. Chem. 1996, 24, 57-109.
- (10) Heger, D.; Eugene, A. J.; Parkin, S. R.; Guzman, M. I. Crystal structure of zymonic acid and a redetermination of its precursor, pyruvic acid. Acta Crystallogr., Sect. E: Crystallogr. Commun. 2019, 75,
- (11) Eugene, A. J.; Pillar, E. A.; Colussi, A. J.; Guzman, M. I. Enhanced acidity of acetic and pyruvic acids on the surface of water. Langmuir 2018, 34, 9307-9313.
- (12) Guzmán, M. I.; Hildebrandt, L.; Colussi, A. J.; Hoffmann, M. R. Cooperative hydration of pyruvic acid in ice. J. Am. Chem. Soc. 2006, 128, 10621-10624.
- (13) Guzmán, M. I.; Colussi, A. J.; Hoffmann, M. R. Photoinduced oligomerization of aqueous pyruvic acid. J. Phys. Chem. A 2006, 110,
- (14) Guzmán, M. I.; Colussi, A. J.; Hoffmann, M. R. Photogeneration of distant radical pairs in aqueous pyruvic acid glasses. J. Phys. Chem. A **2006**, 110, 931-935.
- (15) Guzmán, M. I.; Hoffmann, M. R.; Colussi, A. J. Photolysis of pyruvic acid in ice: Possible relevance to CO and CO2 ice core record anomalies. J. Geophys. Res. D Atmos. 2007, 112, D10123.
- (16) Eugene, A. J.; Guzman, M. I. Reactivity of ketyl and acetyl radicals from direct solar actinic photolysis of aqueous pyruvic acid. J. Phys. Chem. A 2017, 121, 2924-2935.
- (17) Eugene, A. J.; Guzman, M. I. Reply to Comment on "Reactivity of Ketyl and Acetyl Radicals from Direct Solar Actinic Photolysis of Aqueous Pyruvic Acid". J. Phys. Chem. A 2017, 121, 8741-8744.
- (18) Eugene, A. J.; Xia, S.-S.; Guzman, M. I. Negative production of acetoin in the photochemistry of aqueous pyruvic acid. Proc. Natl. Acad. Sci. U.S.A. 2013, 110, E4274-E4275.

- (19) Rapf, R. J.; Perkins, R. J.; Dooley, M. R.; Kroll, J. A.; Carpenter, B. K.; Vaida, V. Environmental processing of lipids driven by aqueous photochemistry of α -keto acids. ACS Cent. Sci. 2018, 4, 624–630.
- (20) Lin, G.; Sillman, S.; Penner, J. E.; Ito, A. Global modeling of SOA: the use of different mechanisms for aqueous-phase formation. Atmos. Chem. Phys. 2014, 14, 5451-5475.
- (21) Physical Constants of Organic Compunds. In CRC Handbook of Chemistry and Physics, 97th ed.; Haynes, W. M., Ed.; CRC Press/Taylor & Francis: Boca Raton, FL, 2017.
- (22) Leermakers, P. A.; Vesley, G. F. The photochemistry of α -keto acids and α -keto esters. I. Photolysis of pyruvic acid and benzoylformic acid. J. Am. Chem. Soc. 1963, 85, 3776-3779.
- (23) Rapf, R. J.; Dooley, M. R.; Kappes, K.; Perkins, R. J.; Vaida, V. pH Dependence of the Aqueous Photochemistry of α -Keto Acids. *J. Phys.* Chem. A 2017, 121, 8368-8379.
- (24) Fischer, M.; Warneck, P. The dissociation constant of pyruvic acid: Determination by spectrophotometric measurements. Ber. Bunsen-Ges. 1991, 95, 523-527.
- (25) Eugene, A.; Guzman, M. The effects of reactant concentration and air flow rate in the consumption of dissolved O2 during the photochemistry of aqueous pyruvic acid. Molecules 2019, 24, 1124.
- (26) Anastasio, C.; McGregor, K. G. Chemistry of fog waters in California's Central Valley: 1. In situ photoformation of hydroxyl radical and singlet molecular oxygen. Atmos. Environ. 2001, 35, 1079-
- (27) Faust, B. C.; Allen, J. M. Aqueous-phase photochemical sources of peroxyl radicals and singlet molecular oxygen in clouds and fog. J. Geophys. Res. D Atmos. 1992, 97, 12913-12926.
- (28) Stockwell, C. E.; Veres, P. R.; Williams, J.; Yokelson, R. J. Characterization of biomass burning emissions from cooking fires, peat, crop residue, and other fuels with high-resolution proton-transferreaction time-of-flight mass spectrometry. Atmos. Chem. Phys. 2015, 15,
- (29) Schwarzenbach, R. P.; Gschwend, P. M.; Imboden, D. M. Environmental Organic Chemistry, 2nd ed.; John Wiley & Sons: Hoboken, NJ, USA, 2003.
- (30) Rincón, A. G.; Guzmán, M. I.; Hoffmann, M. R.; Colussi, A. J. Optical absorptivity versus molecular composition of model organic aerosol matter. J. Phys. Chem. A 2009, 113, 10512-10520.
- (31) Eugene, A. J.; Xia, S.-S.; Guzman, M. I. Aqueous photochemistry of glyoxylic acid. J. Phys. Chem. A 2016, 120, 3817-3826.
- (32) Zhou, R.; Guzman, M. I. CO₂ reduction under periodic illumination of ZnS. J. Phys. Chem. C 2014, 118, 11649-11656.
- (33) Zhou, R.; Guzman, M. I. Photocatalytic Reduction of Fumarate to Succinate on ZnS Mineral Surfaces. J. Phys. Chem. C 2016, 120,
- (34) Aguirre, M. E.; Zhou, R.; Eugene, A. J.; Guzman, M. I.; Grela, M. A. Cu₂O/TiO₂ Heterostructures for CO₂ Reduction Through a Direct Z-scheme: Protecting Cu₂O from Photocorrosion. Appl. Catal., B 2017,
- (35) Xia, S.-S.; Eugene, A. J.; Guzman, M. I. Cross photoreaction of glyoxylic and pyruvic acids in model aqueous aerosol. J. Phys. Chem. A 2018, 122, 6457-6466.
- (36) Görner, H.; Kuhn, H. J. Photodecarboxylation of phenylglyoxylic acid: Influence of para-substituents on the triplet state properties. J. Chem. Soc., Perkin Trans. 2 1999, 2671-2680.
- (37) Mekic, M.; Brigante, M.; Vione, D.; Gligorovski, S. Exploring the ionic strength effects on the photochemical degradation of pyruvic acid in atmospheric deliquescent aerosol particles. Atmos. Environ. 2018, 185, 237-242.
- (38) Webster, G. K.; Kumar, S. Expanding the analytical toolbox: Pharmaceutical application of quantitative NMR (q-NMR). Anal. Chem. 2014, 86, 11474-11480.
- (39) Appiani, E.; Ossola, R.; Latch, D. E.; Erickson, P. R.; McNeill, K. Aqueous singlet oxygen reaction kinetics of furfuryl alcohol: effect of temperature, pH, and salt content. Environ. Sci.: Processes Impacts 2017, 19, 507-516.

- (40) Zhou, X.; Mopper, K. Determination of photochemically produced hydroxyl radicals in seawater and freshwater. Mar. Chem. 1990, 30, 71-88.
- (41) Charbouillot, T.; Brigante, M.; Mailhot, G.; Maddigapu, P. R.; Minero, C.; Vione, D. Performance and selectivity of the terephthalic acid probe for OH as a function of temperature, pH and composition of atmospherically relevant aqueous media. J. Photochem. Photobiol., A **2011**, 222, 70-76.
- (42) Davidson, R. S.; Goodwin, D.; De Violet, P. F. The mechanism of the photo-induced decarboxylation of pyruvic acid in solution. Chem. Phys. Lett. 1981, 78, 471-474.
- (43) Reed Harris, A. E.; Ervens, B.; Shoemaker, R. K.; Kroll, J. A.; Rapf, R. J.; Griffith, E. C.; Monod, A.; Vaida, V. Photochemical kinetics of pyruvic acid in aqueous solution. J. Phys. Chem. A 2014, 118, 8505-
- (44) Aziz, H. R.; Singleton, D. A. Concert along the edge: Dynamics and the nature of the border between general and specific acid-base catalysis. J. Am. Chem. Soc. 2017, 139, 5965-5972.
- (45) Guzmán, M. I.; Colussi, A. J.; Hoffmann, M. R. Photogeneration of distant radical pairs in aqueous pyruvic acid glasses. J. Phys. Chem. A **2006**, 110, 931-935.
- (46) Jones, M.; Fleming, S. A. Organic Chemistry, 4th ed.; W. W. Norton & Company Inc.: New York, NY, USA, 2010; p 1220.
- (47) Grygoryeva, K.; Ončák, M.; Pysanenko, A.; Fárník, M. Pyruvic acid proton and hydrogen transfer reactions in clusters. Phys. Chem. Chem. Phys. 2019, 21, 8221.
- (48) Capozzi, A.; Karlsson, M.; Petersen, J. R.; Lerche, M. H.; Ardenkjaer-Larsen, J. H. Liquid-state ¹³C polarization of 30% through photoinduced nonpersistent radicals. J. Phys. Chem. C 2018, 122, 7432-7443.
- (49) Herrmann, H.; Schaefer, T.; Tilgner, A.; Styler, S. A.; Weller, C.; Teich, M.; Otto, T. Tropospheric aqueous-phase chemistry: Kinetics, mechanisms, and its coupling to a changing gas phase. Chem. Rev. 2015, 115, 4259-4334.
- (50) Kaur, R.; Anastasio, C. Light absorption and the photoformation of hydroxyl radical and singlet oxygen in fog waters. Atmos. Environ. 2017, 164, 387-397.

Supporting Information For:

Production of Singlet Oxygen (${}^{1}O_{2}$) During the Photochemistry of Aqueous Pyruvic Acid: The Effects of pH and Photon Flux under Steady State $O_{2}(aq)$

Concentration

Publication Year: 2019

Alexis J. Eugene and Marcelo I. Guzman*

Department of Chemistry, University of Kentucky, Lexington, Kentucky 40506, USA

*Corresponding author's email: marcelo.guzman@uky.edu

Environmental Science & Technology

| Content | Page |
|--|------|
| Monitoring of hydroxyl radicals | S2 |
| Figure S1. Furfuryl alcohol decay from the photolysis of 0.10 M pyruvic acid at pH 1.0 | S3 |
| Figure S2. Stability of the HO [•] traps benzoic and terephthalic acids during photolysis | S3 |
| References | S3 |

Monitoring of Hydroxyl Radicals (HO*). The hypothetical production of HO* is explored while monitoring photoreactions spiked to [benzoic acid]_{final} = 1.06 mM^{1,2} or [terephthalic acid]_{final} = 0.50 mM.³ Benzoic and terephthalic acids (both purchased from Acros, \geq 99.0%) are known to trap HO* forming o-, m-, and p- hydroxybenzoic acids^{1, 2} and 2-hydroxyterephthalic acid,³ respectively. Each unreacted trap was separated from its hydroxylated product(s) by HPLC using the same column and gradient conditions described above for FFA. The UV detector allowed monitoring the decay of benzoic acid at λ = 218 nm or terephthalic acid at λ = 243 nm. No HO* production was observed using either probe with limits of detection (LOD) for the steady state concentration of hydroxyl radical, [HO*]_{ss}, LOD = 1.3 × 10⁻²⁰ M for benzoic acid and LOD = 1.4 × 10⁻²⁰ M for terephthalic acid. Thus, the production of HO* as a contributing process during the photolysis of aqueous PA can be disregarded during photolysis. Furthermore, no hydroxylated products were detected and Figure S2 (Supporting Information) shows that the concentrations of benzoic and terephthalic acids remained constant during irradiation experiments in the presence of each HO* trap.

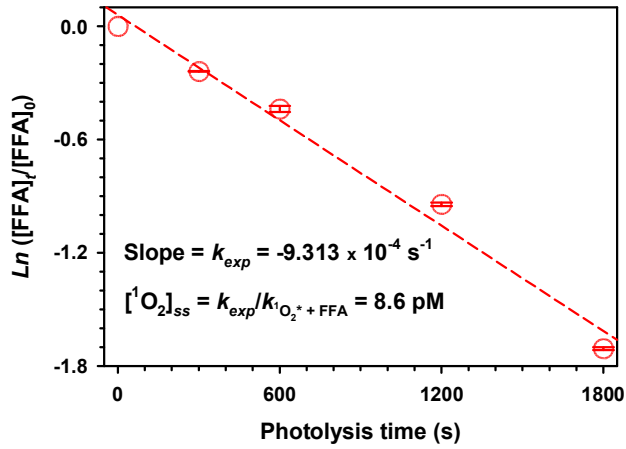


Figure S1. Decay of furfuryl alcohol (FFA) during the photolysis of air saturated 100.0 mM pyruvic acid solutions at pH 1.0 and 25 °C under continuous air sparging using a 25 μ m internal diameter (ID) sparger. The slope is the experimental rate constant for FFA + $^{1}O_{2}^{*}$, k_{exp} .

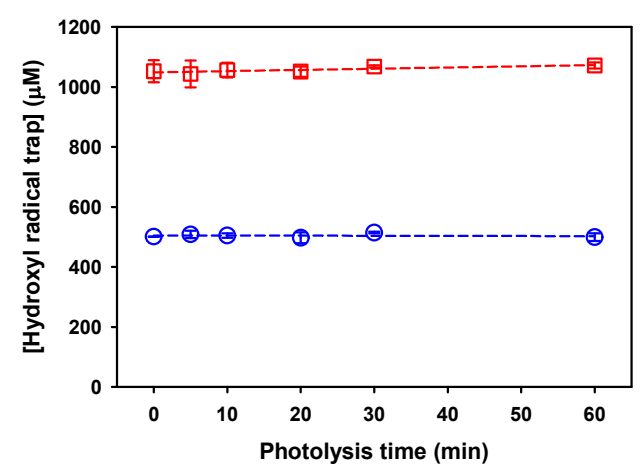


Figure S2. Concentration of the hydroxyl radical trap in experiments using (red square) benzoic acid or (blue circle) terephthalic acid versus time during 1 h photolyses ($\lambda \ge 305$ nm and effective photon flux $I_0 = 1.13 \times 10^{-5}$ Einstein L⁻¹ s⁻¹) of air saturated 100.0 mM pyruvic acid solutions at pH 1.0 and 25 °C under continuous air sparging using a 25 μm internal diameter (ID) sparger.

References

- (1) Zhou, X.; Mopper, K., Determination of photochemically produced hydroxyl radicals in seawater and freshwater. *Mar. Chem.* **1990**, *30*, 71-88.
- (2) Anastasio, C.; McGregor, K. G., Chemistry of fog waters in California's Central Valley: 1. In situ photoformation of hydroxyl radical and singlet molecular oxygen. *Atmos. Environ.* **2001**, *35*, (6), 1079-1089.
- (3) Charbouillot, T.; Brigante, M.; Mailhot, G.; Maddigapu, P. R.; Minero, C.; Vione, D., Performance and selectivity of the terephthalic acid probe for OH as a function of temperature, pH and composition of atmospherically relevant aqueous media. *J. Photoch. Photobio. A* **2011**, 222, (1), 70-76.